Structure and Lattice Dynamics of $La_2Zr_2O_7$ Crystal: Ab Initio Calculation

V. A. Chernyshev(✉)

Ural Federal University, Mira St. 19, 620002 Ekaterinburg, Russia
vchern@inbox.ru

Abstract. Crystal structure and phonon spectrum of rare-earth zirconate $La_2Zr_2O_7$ as well as the whole row $R_2Zr_2O_7$ (R = La, Ce, Pr, Nd, Sm, Eu, Gd, Tb, Dy, Ho, Er, Tm, Yb, Lu) were studied within the framework of density functional theory and MO LKAO approach. The calculations were performed by using hybrid functionals that take into account both local and nonlocal (at the Hartree-Fock formalism) exchanges. Calculations were performed with the most used functionals B3LYP and PBE0. The calculations were also carried out with the functional PBESOL0. The fundamental vibration frequencies of $R_2Zr_2O_7$ were calculated. The calculations were performed in the CRYSTAL17 program designed to simulate periodic structures.

Keywords: Phonon spectrum · Ab initio · DFT · Hybrid functionals

1 Introduction

The interest to the study of rare earth zirconate $R_2Zr_2O_7$ (R is a rare earth ion) is due to the varies of their properties and diverse applications [1–6]. Lanthanum zirconate $R_2Zr_2O_7$ was experimentally investigated by methods of X-ray diffraction, Raman and IR spectroscopy [7–14]. The phonon spectra of other crystals from this series are much less studied [14, 15]. For most crystals the information about the experimental study of their IR and Raman spectra is absent in the research papers. Modeling of the lanthanium zirconate $La_2Zr_2O_7$ and some other crystals from the row were previously performed in the plane waves basis [16–18]. The band structure and elastic properties were calculated in the works [16–18], however the phonon spectrum was not studied. In the last few years the structural phase transitions in rare-earth zirconates were investigated by X-ray structural analysis and Raman spectroscopy [15, 19]. This is relevant to do an ab initio study of the crystal structure and IR and Raman spectra of whole row $R_2Zr_2O_7$ (R = La-Lu) within the framework of a unified approach. In this work the structure and dynamics of crystals $R_2Zr_2O_7$ (R = La-Lu) with the pyrochlore structure ($Fd\bar{3}m$) are investigated in the framework of the MO LCAO approach with hybrid DFT functionals.

© Springer Nature Switzerland AG 2019
S. Misra et al. (Eds.): ICCSA 2019, LNCS 11622, pp. 625–638, 2019.
https://doi.org/10.1007/978-3-030-24305-0_46

2 Calculations

Ab initio calculations were performed within the framework of the density functional theory (DFT) by using hybrid functionals which take into account both local and non-local (in the Hartree-Fock formalism) exchange. Calculations were performed with WC1LYP [20], HSE06 [21, 22], B3LYP [23], PBE0 [24], functionals which have been widely used at the last years [25], as well as with the PBESOL0 functional, which is incremented in the program CRYSTAL17 [26, 27]. By using the hybrid functionals that take into account both local and non-local (HF) exchanges, we can well describe the band structure, IR and Raman spectra, and elastic properties of compounds with an ion-covalent bond [20, 28]. Comparison of B3LYP, PBE0 and other functionals with CCSD calculations has been performed recently (128 functionals of different levels were tested) [29]. It was shown that PBE0 is characterized by a rather small error for functionals of its level relative to the CCSD calculation when reproducing electron density and other parameters [29]. By using the PBE0 hybrid functional we successfully described the structure and dynamics of the crystal lattice of rare-earth titanates with the pyrochlore structure $R_2Ti_2O_7$ (R – rare-earth ion) in our previous work [30]. The coordinates of the ions in the unit cell of zirconates $R_2Zr_2O_7$ with the pyrochlore structure ($Fd\bar{3}m$) are given in Table 1.

Table 1. Ion coordinates in the $R_2Zr_2O_7$ unit cell.

Ion	*x*	*y*	*z*	Wyckoff position
Zr	0	0	0	16*c*
R	1/2	1/2	1/2	16*d*
O1	*x*	1/8	1/8	48*f*
O2	3/8	3/8	3/8	8*b*

Oxygen is included in all structural units of this compound. It is located in two symmetrically nonequivalent positions. Therefore, the reproduction of the structure and properties will depend essentially on the oxygen basis. The basis of TZVP type was used in this work [31]. This basis available on the website of CRYSTAL code [32]. Zirconium basis [33] available on CRYSTAL website also. This basis was used by the authors of the CRYSTAL program to calculate the structure and IR spectrum of zirconium complexes with oxygen ligands [33]. Quasi-relativistic pseudopotentials ECPnMWB were used to describe the inner shells of rare-earth ions (ECP – "effective core potential"; n – the number of internal electrons replaced by a pseudopotential; WB – "quasi-relativistic") [34, 35]. Accordingly, for La n = 46, for Ce n = 47, etc. That is, n = Z-11, where Z is the number of the element in the periodic table. Thus, the inner shells of rare-earth ions were replaced by a pseudopotential on the 4f inclusive. TZVP type valence basis sets «ECP46MWB-II» were used to describe the outer shells, $5s^25p^6$, involved in the formation of a chemical bond [34, 36, 37]. These pseudopotentials and valence basis sets are available on the Stuttgart website [38]. Gaussian primitives with exponent values less than 0.1 were removed from the valence basis sets.

The last diffuse orbital of the f- type was also removed from the valence basis sets. The sequence of calculations was the follow. The optimization of the crystal structure was carried out first. After that the phonon spectrum (or the elastic constants) was calculated for the crystal structure corresponding to the minimum energy. The accuracy of self-consistently solving of the system of Kohn-Sham equations was set at 10^{-10} a.u. (TOLDEE = 10). The parameters "TOLINTEG", determining the accuracy of the calculation of the two-electron integrals were set equal to 8,8,8,8,16. The Monkhorst-Pack shrinking factor was taken to be 8. The phonon spectrum in the CRYSTAL program is calculated at the harmonic approximation. By calculating the Hessian matrix the first derivatives were calculated analytically, while the second derivatives were calculated numerically. The Born charges were used by calculations of the Raman and infrared intensities at CRYSTAL code [39]. Electric dipole properties were calculated by using a periodic Coupled-perturbed Hartree-Fock (CPHF) or Kohn-Sham (CPKS) approach [40–42]. Details of the calculation algorithms are considered in [43].

3 Results and Discussion

The crystal structure of $La_2Zr_2O_7$ was calculated with various hybrid functionals. The results are shown in Table 2. Hybrid functionals reproduce the crystal structure of lanthanum zirconate quite well. Functional HSE06 [21] gives quite a good result. Apparently, the separation of the exchange contribution into the short-range ("SR") and long-range ("LR") in HSE06 has been done successfully. This approximation saves the computer resources. The calculation of the crystal structure with the HSE06 functional requires 5 times less time than the calculation with the PBE0 functional. Such a reduction in computer costs only slightly worsens the discrepancy with the experiment (Table 2). The PBESOL0 functional differs from PBE0. Instead of the local exchange-correlation functional PBE it uses PBESOL [44]. The calculation with PBESOL0 functional underestimates the lattice constant. The discrepancy with the experiment at absolute value is comparable with the PBE0 calculation (Table 2). The B3LYP functional gives the maximum discrepancy with the experiment (Table 2), which may be associated with a smaller percentage of the HF exchange. The crystal structure for the all row $R_2Zr_2O_7$ (R = La-Lu) was calculated with the PBE0 functional, as well as with the PBESOL0 functional (Tables 3, 4 and 5). The calculation results are in good agreement with the experiment [2, 14, 45, 46]. The "Difference" column in Tables 3, 4 and 5 shows the change of the values at the La-Lu row. The information of the distances from rare-earth ion to ligands (Table 5) may be useful for crystal field calculation on the rare-earth ion.

According to calculations, the x coordinate increases slightly in the row La-Lu (Table 4). In the pyrochlore structure the rare-earth ion is surrounded by eight oxygen ions, two of which are at a certain distance and six are at another distance.

Table 2. The lattice constant, interionic distances (Å), x coordinate of oxygen O1 (relative units) at $La_2Zr_2O_7$. The percentage of HF-exchange is given in parenthesis after the name of the functional.

Hybrid functional	WC1LYP (16%)	HSE06 (25%)	B3LYP (20%)	PBE0 (25%)	PBESOL0 (25%)	Exp. [8]	Exp. [9]
Lattice constant	10.885	10.841	10.940	10.838	10.763	10.798 (3)	10.805
La–O1	2.65	2.64	2.67	2.64	2.62	2.63 (3)	–
La–O2	2.3567	2.3472	2.3685	2.3465	2.3303	2.3379 (9)	–
Zr-O1	2.124	2.116	2.132	2.115	2.103	2.105 (18)	–
La-Zr	3.8485	3.8330	3.8678	3.8318	3.8054	3.8178 (13)	–
x	0.333	0.333	0.332	0.333	0.333	–	0.332

Table 3. Lattice constant of $R_2Zr_2O_7$ (R = La-Lu), Å

R	PBE0	PBESOL0	Exp. [14]	Exp. [45]	Exp. [46]	Exp. [47]
La	10.8379	10.7633	10.805	10.7992 (1)		
Ce	10.7985	10.7234			10.7135 (1)	
Pr	10.7618	10.6872	10.715	10.7010 (1)		
Nd	10.7266	10.6526	10.678	10.6134 (1)		10.6611 (1)
Sm	10.6657	10.5896	10.594	10.5907 (1)		
Eu	10.6348	10.5589	10.554			
Gd	10.6092	10.5333	10.528	10.5341 (1)		
Tb	10.5818	10.5058	10.476			
Dy	10.5554	10.4792	10.450			
Ho	10.5304	10.4543	10.419			
Er	10.5060	10.4309	10.395			
Tm	10.4848	10.4102	10.368			
Yb	10.4623	10.3869	10.336			
Lu	10.4508	10.3763				
Difference	0.3871	0.3870	0.469			

The parameter ρ (Table 5), which characterizes the distortion of the oxygen environment of the rare-earth ion, according to [47], is equal to:

$$\rho = \frac{R - O2}{R - O1}$$

The closer ρ is to one, the less there is distortion. According to the calculations, the distortion decreases in the La-Lu series. The change of the R-O1 and R-O2 distances in the row is shown at Fig. 1. The results of the bandgap calculation are shown in Table 6. The calculations predict a straight (Γ-Γ) bandgap for the all row La-Lu. Note that the experimental bandgap value for a thin film of $La_2Zr_2O_7$ is 4.96–5.60 eV [48], which agrees with the calculations quite well. According to the calculations, the bandgap value decreases almost linearly in the La-Lu series.

Table 4. *x* coordinate of oxygen O1 (48*f*) at $R_2Zr_2O_7$ (R = La-Lu), relative units.

R	PBE0	PBESOL0	Exp.
La	0.3327	0.3332	0.332 [9]
Ce	0.3336	0.3342	
Pr	0.3345	0.3351	
Nd	0.3353	0.3359	0.3357 (2) [46]
Sm	0.3369	0.3375	
Eu	0.3376	0.3383	
Gd	0.3383	0.3390	
Tb	0.3390	0.3398	
Dy	0.3397	0.3404	
Ho	0.3404	0.3411	
Er	0.3411	0.3418	
Tm	0.3416	0.3424	
Yb	0.3422	0.3430	
Lu	0.3425	0.3433	
Difference	0.0098	0.0101	

Table 5. Interionic distances R-O at $R_2Zr_2O_7$ (R = La-Lu), Å. It is PBESOL0 calculation.

R	R-O2 × 2	R-O1 × 6	ρ
La	2.330	2.615	0.891
Ce	2.322	2.599	0.893
Pr	2.314	2.584	0.896
Nd	2.306	2.569	0.898
Sm	2.293	2.543	0.902
Eu	2.286	2.530	0.904
Gd	2.281	2.519	0.905
Tb	2.275	2.507	0.907
Dy	2.269	2.496	0.909
Ho	2.263	2.485	0.911
Er	2.258	2.475	0.913
Tm	2.254	2.466	0.914
Yb	2.249	2.456	0.916
Lu	2.247	2.451	0.917
Difference	0.083	0.064	0.026

Rare-earth zirconates $R_2Zr_2O_7$ (R = La-Lu) with pyrochlore structure have phonon modes at the Γ point:

$$\Gamma = A_{1g} + E_g + 2F_{1g} + 4F_{2g} + 3A_{2u} + 3E_u + 8F_{1u} + 4F_{2u}.$$

Here A_{1g}, E_g and $4F_{2g}$ are Raman active modes, $7F_{1u}$ are infrared active modes, 4F2u, 3Eu, 2F1 g, 3A2u are silent modes. The results of the calculation of phonon

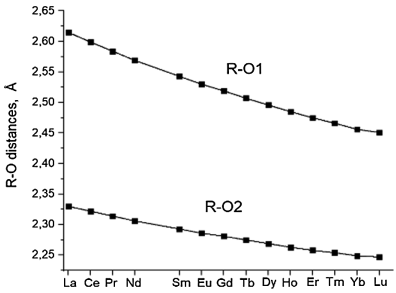


Fig. 1. The distances R-O at the row $R_2Zr_2O_7$ (R = La-Lu)

Table 6. Bandgap value (eV) at the row $R_2Zr_2O_7$ (R = La-Lu). It is PBE0 calculation.

La	Ce	Pr	Nd	Sm	Eu	Gd
6.19	6.11	6.01	5.96	5.79	5.71	5.64
Tb	Dy	Ho	Er	Tm	Yb	Lu
5.56	5.49	5.41	5.34	5.26	5.19	5.15

modes at the Γ point of $La_2Zr_2O_7$ are given in Table 7. Frequencies and types of the phonon modes were determined from the ab initio calculation. From the analysis of displacement vectors obtained from this ab initio calculations, the degree of participation of each ion in a particular mode is estimated. The ions that are shifted anyway significantly in the mode are listed in the column "Ion-participants". The "S" index is a strong shift ("Strong"), "W" is weak ("Weak"). We can distinguish modes in which only oxygen ions are involved. Only oxygen ions are involved in the infrared active mode F1u with a frequency of $\sim$245 cm^{-1}. O1 ions, located at 48*f* position, characterized by the x coordinate, participate mainly in this mode. O1 is also predominantly involved in the most intense Raman mode F_{2g} ($\sim$310 cm^{-1}). Only O1 ions are involved in the Raman Eg mode. According to calculations, this is the second most intense mode in the Raman spectrum (Table 7, Fig. 2). Only O1 ions also participate in the Raman modes A_{1g} and the high-frequency F_{2g}. Thus, the behavior of these modes gives information about the value of the x coordinate of the oxygen O1 under external influences on the crystal. The oxygen O2, located at 8*b* position, mainly participates in F_{2g} modes with frequencies of $\sim$420 and $\sim$540 cm^{-1}. All ions are involved in IR active modes (F1u), but they participate in varying degrees. Zirconium and both O1 and O2 oxygens are involved in the most intense F1u mode with a frequency of $\sim$330 cm^{-1}, moreover, as oxygen O1 taking the most participation. At the low-frequency F1u mode ($\sim$100 cm^{-1}) all ions are involved, but mainly zirconium is involved. It may be noted that lanthanum and zirconium are significantly involved in silent modes. At an experimental work [12] the participation of the structural units La-O and ZrO_6 in the Raman modes with frequencies of 299 and 506 cm^{-1} ("stretching modes") was discussed. This is consistent with the fact that the calculation predicts a strong displacement of O1 oxygen in these modes and the participation of O2 oxygen (Table 7). The calculation results are also consistent with the experiment [13], where

the intense IR modes 366 and 508 cm^{-1} were found, for which the calculation predicts a strong participation of O1 oxygen, i.e. change of Zr-O bond length. The results of modeling the Raman spectrum of the $La_2Zr_2O_7$ based on the calculated frequencies and intensities for the polycrystal are shown at Fig. 2. The Pseudo-Voigt functions with a damping factor of 8 cm^{-1} were used by modeling. The results agree well not only with the Raman spectrum measured at T = 298 K, but also with the spectrum measured at T = 1400 K. The results of the simulation of the IR spectrum are shown at Fig. 3. The presence of two peaks near to 350 and 500 cm^{-1} agrees well with the results of measuring the transmittance of the IR spectrum of $La_2Zr_2O_7$ [13].

Table 7. Frequencies (cm^{-1}) and types of phonon modes at the Γ point. The intensity of IR modes (km/mol) is given in parentheses. The abbreviations in the "R" (Raman) and "IR" columns: "A" is an active mode, "I" is inactive one.

Type	IR	R	Frequency, calculation		Frequency, experiment					Ions-participants
					[10] (IR)	[11] (IR)	[12] (R, IR)	[13] (IR)	[14] (IR)	
			PBE0	PBE SOL0						
F_{2u}	I	I	54	62						La^S, Zr^W, $O1^W$
E_u	I	I	96	99						La, Zr, O1
F_{1u}	A	I	101 (180)	105 (48)	101	104.8				La, Zr^S, O1, O2
F_{2u}	I	I	130	136						La, Zr^S, O1
F_{1u}	A	I	137 (1781)	142 (1589)	140	141.5				La^S, Zr, $O1^S$
E_u	I	I	146	154						La, Zr, $O1^S$
F_{1u}	A	I	202 (6812)	206 (6577)	176	166.8			215	La, Zr, $O1^S$
F_{1u}	I	I	245 (152)	249 (26)	244; 208	213.7			245	$O1^S$, O2
A_{2u}	A	I	250	259						La, Zr, O1
F_{1g}	I	I	256	264						$O1^S$
F_{2u}	I	I	281	287						Zr^W, $O1^S$
A_{2u}	I	I	301	306						La, Zr^S
F_{2g}	I	A	308	318			299			$O1^S$, O2
E_g	I	A	324	334						$O1^S$
F_{1u}	A	I	328 (16143)	341 (16244)	352	352.7		366		La^W, Zr, $O1^S$, O2
F_{1u}	A	I	383 (1.07)	396 (0.02)	412	411.9			370	La, O1, $O2^S$
A_{2u}	I	I	390	392						La^W, Zr^S, $O1^S$
E_u	I	I	393	400						La^W, Zr^W, $O1^S$
F_{2g}	I	A	413	421						O1, $O2^S$
F_{1u}	A	I	499 (2869)	508 (3354)	518	517.4	508	508	505	Zr^W, $O1^S$, O2
A_{1g}	I	A	505	510			506			$O1^S$
F_{2g}	I	A	535	545						O1, $O2^S$
F_{1g}	I	I	556.6	571						$O1^S$
F_{2u}	I	I	557.1	570						$O1^S$
F_{2g}	I	A	757	768						$O1^S$

Note. The "S" index is a strong shift ("Strong"), "W" is weak ("Weak") at the last column.

The results of the intensity calculation of the Raman modes for the polycrystal and single crystal $La_2Zr_2O_7$ are given in Tables 8 and 9 (PBE0 calculation).

Table 8. Raman modes intensity for polycrystalline sample $La_2Zr_2O_7$ (relative units). The intensity of the Raman modes was calculated for λ = 488 nm and T = 298 K.

Type	Frequency, cm^{-1}	I_{tot}	I_{par}	I_{perp}
F_{2g}	308	1000	571	429
E_g	325	219	125	94
F_{2g}	413	17	10	7
A_{1g}	506	45	45	0
F_{2g}	536	77	44	33
F_{2g}	758	27	15	12

Table 9. Raman modes intensity for single crystal $La_2Zr_2O_7$ (relative units). The intensity of the Raman modes was calculated for λ = 488 nm and T = 298 K.

Type	Frequency, cm^{-1}	I *xx*	I *xy*	I *xz*	I *yy*	I *yz*	I *zz*
F_{2g}	308	0	1000	1000	0	1000	0
E_g	325	438	0	0	438	0	438
F_{2g}	413	0	17	17	0	17	0
A_{1g}	506	63	0	0	63	0	63
F_{2g}	536	0	77	77	0	77	0
F_{2g}	758	0	27	27	0	27	0

The results of calculating the IR and Raman modes for the all row $R_2Zr_2O_7$ (R = La-Lu) are given in Tables 10, 11 and 12 as well as at Figs. 4 and 5. The frequencies of low-frequency F_{2g} modes slightly decrease in the La-Lu row. While the frequency of the high-frequency F_{2g} mode increases significantly (Table 10, Fig. 4). The frequencies of the IR modes in the La-Lu series vary considerably more than the frequencies of the Raman modes. The frequency of the low-frequency F1u mode decreases, while the frequencies of the high-frequency F1u modes increase (Table 11). The four most strongly varying infrared modes at the row are shown in Fig. 5. The calculation results are in good agreement with the available experimental data. The results of calculating the IR and Raman modes for the all row $R_2Zr_2O_7$ (R = La-Lu) are given in Tables 10, 11 and 12 as well as at Figs. 4 and 5. The frequencies of low-frequency F_{2g} modes slightly decrease in the La-Lu row. While the frequency of the high-frequency F_{2g} mode increases significantly (Table 10, Fig. 4). The frequencies of the IR modes in the La-Lu series vary considerably more than the frequencies of the Raman modes. The frequency of the low-frequency F1u mode decreases, while the frequencies of the high-frequency F1u modes increase (Table 11). The four most strongly varying infrared modes at the row are shown in Fig. 5. The calculation results are in good agreement with the available experimental data.

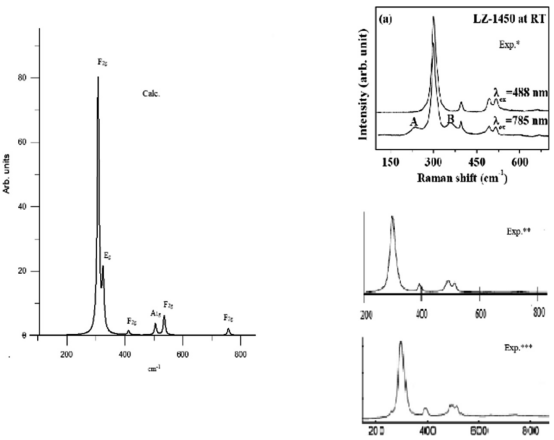


Fig. 2. Calculation results of the $La_2Zr_2O_7$ Raman spectrum (PBE0 calculation). The intensity of the Raman modes was calculated for λ = 488 nm and T = 298 K. At modeling the Raman spectrum based on the calculated frequencies and intensities for a polycrystal, the Pseudo-Voigt functions with a damping factor of 8 cm^{-1} were used. The sidebars show: Exp.* – is experiment [8], performed at λ = 488 nm as well as at λ = 785 nm and T = 298 K. Exp.** – is experiment [7], performed at λ = 488 nm and T = 298 K. Exp.***– is experiment [3], performed at λ = 532 nm and T = 1400 K.

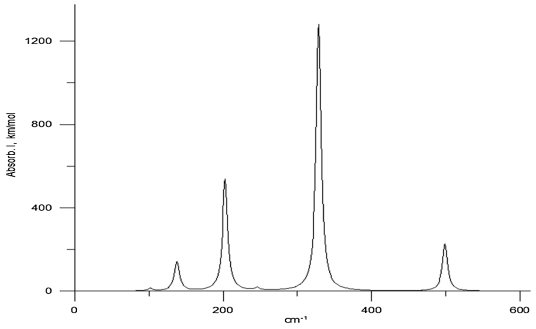


Fig. 3. Calculation results of the IR spectrum of $La_2Zr_2O_7$ (PBE0 calculation). All infrared modes are F_{1u} type.

The results of the calculation of the elastic constants and the bulk modulus are given in Table 13. The results are in good agreement with the calculations of the elastic constants in the plane-wave basis [16]. Experimental data by the elastic constants of $R_2Zr_2O_7$ (R = La-Lu) in the scientific publications could not be found.

Table 10. Raman modes of $R_2Zr_2O_7$ (R = La-Lu). Frequencies are at cm^{-1} (PBE0 calculation). Experiments data [15] are in parenthesis.

R	F_{2g}	F_{2g}	F_{2g}	F_{2g}	E_g	A_g
La	308	413	535	757	324	505
Ce	309	413	536	762	326	507
Pr	309	414	536	767	327	509
Nd	309	414	537	771	328	511
Sm	309	414	537	778	330	514
Eu	308	414	537	782	331	515
Gd	308	414	537	785	332	516
Tb	307	413	537	788	332	518
Dy	307 (∼300)	413	537	792	333	519 (∼520)
Ho	306	413	538	794	334	520
Er	305	412	538	797	335	521
Tm	304	412	538	800	335	522
Yb	304	411	538	803	336	523
Lu	303	411	539	804	336	524
Difference	6	3	4	67	12	19

Table 11. Infrared modes of $R_2Zr_2O_7$ (R = La-Lu). Frequencies are at cm^{-1} (PBE0 calculation). All modes are F1u type. Experiments data [14] are in parenthesis.

La	101	137	202 (215)	245 (245)	328	383 (370)	499 (505)
Ce	100	135	201	242	331	386	503
Pr	99	133	200 (215)	238	332 (365)	388 (400)	508 (530)
Nd	98	131	199 (215)	234	333 (365)	391 (400)	512 (525)
Sm	94	125	195	227 (225)	333	396 (420)	519 (530)
Eu	92	123	194	223 (225)	334	399 (420)	523 (525)
Gd	91	120	193	220 (225)	334	402 (420)	526 (510)
Tb	89	117	191	215	334	405 (420)	529 (500)
Dy	87	114	189	212	333.4	408 (420)	532
Ho	85	112	187	208	333	411 (420)	535
Er	82	109	186	205	332	413 (420)	538
Tm	81	107	184	201	333	416 (420)	541
Yb	77	103	181	198	332	418 (420)	543
Lu	75	102	180	195	332	420 (440,400)	544
Difference	26	35	22	50	4	37	45

Table 12. Silent modes at the row $R_2Zr_2O_7$ (R = La-Lu). Frequencies are in cm^{-1} (PBE0 calculation).

R	A_{2u}	A_{2u}	A_{2u}	E_u	E_u	E_u	F_{1g}	F_{1g}	F_{2u}	F_{2u}	F_{2u}	F_{2u}
La	250	301	390	96	146	393	256	557	54	131	281	557
Ce	248	302	391	95	141	396	256	562	53	131	283	565
Pr	245	303	391	94	138	399	254	568	52	130	285	572
Nd	242	305	392	93	133	402	253	573	51	130	287	578
Sm	231	306	392	89	125	407	251	580	48	129	292	589
Eu	227	308	393	87	122	409	249	585	47	128	294	595
Gd	222	309	393	85	119	412	248	588	46	128	297	600
Tb	218	310	394	83	115	414	247	591	45	128	299	604
Dy	213	312	394	80	113	416	245	595	43	127	301	609
Ho	210	313	395	77	111	419	244	599	42	127	304	614
Er	205	318	399	74	112	419	242	601	40	125	306	618
Tm	202	315	396	70	106	423	240	604	38	126	308	622
Yb	197	316	397	66	105	425	238	607	36	126	310	626
Lu	196	316	398	64	105	426	236	608	33	126	311	628
Difference	54	15	8	28	41	31	20	51	21	5	30	71

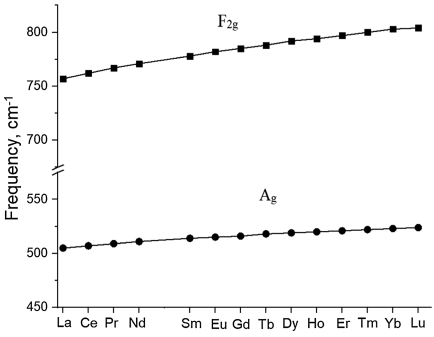


Fig. 4. The Raman modes at the row $R_2Zr_2O_7$ (R = La-Lu). The two most varying Raman modes at the row are shown.

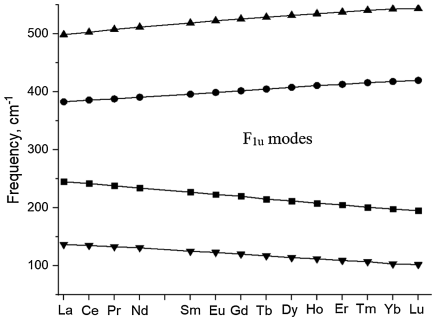


Fig. 5. The infrared modes at the row $R_2Zr_2O_7$ (R = La-Lu). The four most varying infrared modes at the row are shown.

Table 13. Elastic constants and bulk modulus of $R_2Zr_2O_7$ (GPa).

	$La_2Zr_2O_7$		$Gd_2Zr_2O_7$	$Yb_2Zr_2O_7$
	This work (PBE0)	VASP calculation (from work [16])	This work (PBE0)	This work (PBE0)
C_{11}	298.2	289.8	319.4	332.8
C_{12}	116.9	124.8	110.8	105.9
C_4	98.6	100.4	96.0	91.0
B	177.4	179.8	180.33	181.5

4 Conclusion

Ab initio calculation of all row the rare-earth zirconates $R_2Zr_2O_7$ (R = La-Lu) with the pyrochlore structure, carried out within the framework of the MO LCAO approach, with a hybrid DFT functionals that takes into account the contribution of the HF exchange. The calculations reproduce the crystal structure of these compounds in good agreement with the experiment. The calculation of the phonon spectrum of these compounds at the Γ point was carried out for the first time. From the analysis of displacement vectors obtained from this ab initio calculations, the degree of participation of each ion in a particular mode were estimated. It was shown that only oxygen ions are involved in Raman modes. The modes with absolute or predominant participation of oxygen at the 48*f* position, characterized by the displacement x, are determined. The obtained results can be used for interpretation of experimental data on the Raman and IR spectra of rare-earth zirconates with pyrochlore structure.

Acknowledgments. This study was supported by the Ministry of Education and Science of the Russian Federation (project no. 3.9534.2017/8.9).

References

1. Pokhrel, M., Alcoutlabi, M., Mao, Y.: Optical and X-ray induced luminescence from Eu3 + doped $La_2Zr_2O_7$ nanoparticles. J. Alloys Compd. **693**, 719–729 (2017)
2. Hatnean, M.C., Decorse, C., Lees, M.R., Petrenko, O.A., Balakrishnan, G.: Zirconate pyrochlore frustrated magnets: crystal growth by the floating zone technique. Crystals **6**(7), 79 (2016)
3. Popov, V.V., et al.: Features of formation and evolution of crystal and local structures in nanocrystalline $Ln_2Zr_2O_7$ (Ln = La - Tb). J. Phys: Conf. Ser. **941**(1), 012079 (2017)
4. Kong, L., Karatchevtseva, I., Gregg, D.J., Blackford, M.G., Holmes, R., Triani, G.: A novel chemical route to prepare $La_2Zr_2O_7$ Pyrochlore. J. Am. Ceram. Soc. **96**(3), 935–941 (2013)
5. Modeshia, D.R., Walton, R.I.: Solvothermal synthesis of perovskites and pyrochlores: crystallisation of functional oxides under mild conditions. Chem. Soc. Rev. **49**(11), 4303–4325 (2010)
6. Chen, A., Smith, J.R., Duncan, K.L., DeHoff, R.T., Jones, K.S., Wachsman, E.D.: Effect of $La_2Zr_2O_7$ on interfacial resistance in solid oxide fuel cells. J. Electrochem. Soc. **157**(11), B1624–B1628 (2010)

7. Shimamura, K., Arima, T., Idemitsu, K., Inagaki, Y.: Thermophysical properties of rare-earth-stabilized zirconia and zirconate pyrochlores as surrogates for actinide-doped zirconia. Int. J. Thermophysics. **28**(3), 1074–1084 (2007)
8. Paul, B., Singh, K., Jaron, T., Roy, A., Chowdhury, A.: Structural properties and the fluorite–pyrochlore phase transition in $La_2Zr_2O_7$: the role of oxygen to induce local disordered states. J. Alloys Compd. **686**(25), 130–136 (2016)
9. Subramanian, M., Aravamudan, G., Subba Rao, G.: Oxide pyrochlores - a review. Prog. Solid State Chem. **15**(2), 55–143 (1983)
10. Gundovin, N.V., Spiridonov, F.M., Komissarova, L.N., Petrov, K.I.: The vibrational spectra of zirconates and hafnates of rare-earth elements with pyrochlore structure. Zh. Neorg. Khim. **20**, 582–586 (1975)
11. Cheng, X., et al.: Infrared phonon modes and dielectric properties of $La_2Zr_2O_7$: Comparing thin film to bulk material. Phys. Stat. Sol. (b) 249(4), 854–857 (2011)
12. Tong, Y., Wang, Y., Yu, Z., Wang, X., Yang, X., Lu, L.: Preparation and characterization of pyrochlore $La_2Zr_2O_7$ nanocrystals by stearic acid method. Mater. Lett. **62**(6–7), 889–891 (2008)
13. Chen, D., Xu, R.: Hydrothermal synthesis and characterization of $La_2M_2O_7$ (M = Ti, Zr) powders. Mater. Res. Bull. **33**(3), 409–417 (1988)
14. Klee, W.E., Weitz, G.: Infrared spectra of ordered and disordered pyrochlore-type compounds in the series $RE_2Ti_2O_7$, $RE_2Zr_2O_7$ and $RE_2Hf_2O_7$. J. Inorg. Nucl. Chem. **31** (8), 2367–2372 (1969)
15. Rittman, D.R., et al.: Strain engineered pyrochlore at high pressure. Sci. Rep. **7**(1), 2236 (2017)
16. Guo, X., Zhang, J.: First principles study of thermodynamic properties of lanthanum zirconate. Mater. Today Proc. **1**, 25–34 (2014)
17. Feng, J., et al.: Electronic structure, mechanical properties and thermal conductivity of $Ln_2Zr_2O_7$ (Ln = La, Pr, Nd, Sm, Eu and Gd) pyrochlore. Acta Mater. **59**(4), 1742–1760 (2011)
18. Zhang, S., et al.: Impact of isovalent and aliovalent substitution on the mechanical and thermal properties of $Gd_2Zr_2O_7$. Sci. Rep. **7**(1), 6399 (2017)
19. Maram, P.S., Ushakov, S.V., Weber, R.J.K., Benmore, C.J., Navrotsky, A.: In situ diffraction from levitated solids under extreme conditions-structure and thermal expansion in the Eu_2O_3–ZrO_2 system. J. Am. Ceram. Soc. **98**(4), 1292–1299 (2015)
20. Pierre, M.L., Orlando, R., Maschio, L., Doll, K., Ugliengo, P., Dovesi, R.: Performance of six functionals (LDA, PBE, PBESOL, B3LYP, PBE0, and WC1LYP) in the simulation of vibrational and dielectric properties of crystalline compounds. The case of forsterite Mg_2SiO_4. J. Comp. Chem. **32**(9), 1775–1784 (2011)
21. Heyd, J., Scuseria, G.E., Ernzerhof, M.: Hybrid functionals based on a screened Coulomb potential. J. Chem. Phys. **118**(8), 8207–8215 (2003)
22. Benjamin, G.J., Thomas, M.H., Gustavo, E.S.: Screened hybrid density functionals for solid-state chemistry and physics. Phys. Chem. Chem. Phys. **11**(3), 443–454 (2009)
23. Becke, A.D.: Density functional thermochemistry. III. The role of exact exchange. J. Chem. Phys. **98**(7), 5648–5652 (1993)
24. Perdew, J.P., Ernzerhof, M., Burke, K.: Rationale for mixing exact exchange with density functional approximations. J. Chem. Phys. **105**(2), 9982–9985 (1996)
25. Burke, K.: Perspective on density functional theory. J. Chem. Phys. **136**(15), 150901 (2012)
26. Dovesi, R., et al.: 2018 CRYSTAL17 User's Manual. http://www.crystal.unito.it/Manuals/crystal17.pdf
27. Dovesi, R., et al.: Quantum-mechanical condensed matter simulations with CRYSTAL. Comput. Mol. Sci. **8**(4), e1360 (2018)
28. Evarestov, R.A., Bandura, A.V., Aleksandrov, V.E.: Calculations of the electronic structure of crystalline $SrZrO_3$ in the framework of the density-functional theory in the LCAO approximation. Phys. Solid State **47**(12), 2248–2256 (2005)

29. Medvedev, M.G., Bushmarinov, I.S., Sun, J., Perdew, J.P., Lyssenko, K.A.: Density functional theory is straying from the path toward the exact functional. Science **355**(6320), 49–52 (2017)
30. Chernyshev, V.A., Petrov, V.P., Nikiforov, A.E., Agzamova, P.A., Avram, N.M.: Elastic properties of rare earth pyrochlores $R_2Ti_2O_7$ (R = Gd, Tb, Dy, Ho, Er, Tm, Yb, Lu): Ab initio calculations. Opt. Mater. **72**, 565–570 (2017)
31. Peintinger, M.F., Oliveira, D.V., Bredow, T.: Consistent Gaussian basis sets of triple zeta valence with polarization quality for solid state calculations. J. Comp. Chem. **34**(6), 451–459 (2012)
32. CRYSTAL website. http://www.crystal.unito.it/index.php
33. Valenzano, L., et al.: Disclosing the complex structure of UiO-66 metal organic framework: a synergic combination of experiment and theory. Chem. Mater. **23**(7), 1700–1718 (2011)
34. Dolg, M., Stoll, H., Savin, A., Preuss, H.: Energy-adjusted pseudopotentials for the rare earth elements. Theor. Chim. Acta. **75**(3), 173–194 (1989)
35. Dolg, M., Stoll, H., Preuss, H.: A combination of quasirelativistic pseudopotential and ligand field calculations for lanthanoid compounds. Theor. Chim. Acta. **85**(6), 441–450 (1993)
36. Yang, J., Dolg, M.: Valence basis sets for lanthanide 4f-in-core pseudopotentials adapted for crystal orbital ab initio calculations. Theor. Chem. Acc. **113**(4), 212–224 (2005)
37. Weigand, A., Cao, X., Yang, J., Dolg, M.: Quasirelativistic f-in-core pseudopotentials and core-polarization potentials for trivalent actinides and lanthanides: molecular test for trifluorides. Theor. Chem. Acc. **126**(3–4), 117–127 (2009)
38. Energy-consistent Pseudopotentials of the Stuttgart. http://www.tc.uni-koeln.de/PP/clickpse.en.html
39. Maschio, L., Kirtman, B., Orlando, R., Rerat, M.: Ab initio analytical infrared intensities for periodic systems through a coupled perturbed Hartree-Fock/Kohn-Sham method. J. Chem. Phys. **137**(20), 204113 (2012)
40. Maschio, L., Kirtman, B., Rerat, M., Orlando, R., Dovesi, R.: Comment on "Ab initio analytical infrared intensities for periodic systems through a coupled perturbed Hartree-Fock/Kohn-Sham method" [J. Chem. Phys. 137, 204113 (2012)]. J. Chem. Phys. **139**, 164101 (2013)
41. Maschio, L., Kirtman, B., Rerat, M., Orlando, R., Dovesi, R.: Ab initio analytical Raman intensities for periodic systems through a coupled perturbed Hartree-Fock/Kohn-Sham method in an atomic orbital basis. II. Validation and comparison with experiments. J. Chem. Phys. **139**(16), 164102 (2013)
42. Orlando, R., Lacivita, V., Bast, R., Ruud, K.: Calculation of the first static hyperpolarizability tensor of three-dimensional periodic compounds with a local basis set: a comparison of LDA, PBE, PBE0, B3LYP, and HF results. J. Chem. Phys. **132**(24), 244106 (2010)
43. Dovesi, R., et al.: CRYSTAL14: a program for the ab initio investigation of crystalline solids. Int. J. Quant. Chem. **114**(19), 1287–1317 (2014)
44. Perdew, J.P., et al.: Restoring the density-gradient expansion for exchange in solids and surfaces. Phys. Rev. Lett. **100**(13), 136406 (2008)
45. Gao, B., et al.: Experimental signatures of a three-dimensional quantum spin liquid in effective spin-1/2 $Ce_2Zr_2O_7$ pyrochlore (2019). https://arxiv.org/abs/1901.10092
46. Xu, J., et al.: Magnetic structure and crystal-field states of the pyrochlore antiferromagnet $Nd_2Zr_2O_7$. Phys. Rev. B **92**(22), 224430 (2015)
47. Li, X., et al.: Long-range antiferromagnetic order in the frustrated XY pyrochlore antiferromagnet $Er_2Ge_2O_7$. Phys. Rev. B **89**(6), 064409 (2014)
48. Kaspar, T.C., et al.: Damage evolution of ion irradiated defected-fluorite $La_2Zr_2O_7$ epitaxial thin films. Act. Mater. **130**, 111–120 (2017)